





Article

Petrological Features of the Burlakski and Nizhne-Derbinsk Mafic-Ultramafic Plutons (East Sayan Mountains, Siberia, Russia)

Tamara Yakich ^{1,*}, Matthew Brzozowski ², Alexey Chernishov ³, Giovanni Grieco ⁴, Olesya Savinova ¹, Timofey Timkin ¹ and Alexander Marfin ⁵

¹ School of Earth Sciences and Engineering, Division for Geology, Tomsk Polytechnic University, 634050 Tomsk, Russia; logvinenkoov@tpu.ru (O.S.); timkin@tpu.ru (T.T.)

² State Key Laboratory for Mineral Deposits Research, School of Earth Sciences and Engineering, Nanjing University, Nanjing 210023, China; matt.brzozow@gmail.com

³ Department of Petrography, National Research Tomsk State University, 36 Lenin Ave., 634050 Tomsk, Russia; aich@ggf.tsu.ru

⁴ Department of Earth Sciences, Università degli Studi di Milano, via Botticelli 23, 20122 Milan, Italy; giovanni.grieco@unimi.it

⁵ Institute of the Earth's Crust, Siberian Branch of the Russian Academy of Sciences, 664033 Irkutsk, Russia; marfin1309@gmail.com

* Correspondence: cherkasovatu@tpu.ru; Tel.: +7-961-889-07-65

Received: 30 December 2019; Accepted: 27 January 2020; Published: 30 January 2020



Abstract: The Nizhne-Derbinsk mafic-ultramafic complex is located between the Central Asian Orogenic Belt and the Siberian Craton and, is associated with the Ballyk fault. The largest, spatially related to each other, plutons in the central part of the complex are the Burlakski and Nizhne-Derbinsk. Rocks in the main units of these plutons are divided into three groups: peridotites (ultramafic), pyroxenites (sub-ultramafic), and gabbroic rocks (mafic). The ultramafic and sub-ultramafic cumulate series are devoid of plagioclase and contain <3 vol. % chromian spinel. The Fo content of olivine in the sub-ultramafic cumulates from both plutons ranges from Fo79 to Fo86. The En content [= Mg/(Mg + Fe + Ca) × 100 atomic ratio] of clinopyroxenes and orthopyroxenes varies from 46–56, and 63–80, respectively. Plagioclase corresponds to labradorite with An contents between 55 and 57. Hornblende is compositionally similar to pargasite. The sequence of change of rock units corresponds to the paragenesis: olivine – olivine + clinopyroxene (orthopyroxene) – clinopyroxene + orthopyroxene – clinopyroxene + orthopyroxene + plagioclase – orthopyroxene. Petrographic, mineralogical, and mineral chemical features of the Burlakski and Nizhne-Derbinsk plutons suggest that the diversity of the material composition of these plutons is due to the processes of magmatic differentiation in deep-seated conditions. Estimates of crystallization pressures and temperatures of the Burlakski and Nizhne-Derbinsk plutons suggest that they crystallized at high pressures ≥ 10kb and temperatures ranging from 1000–1400 °C. Mineralogical and petrological features suggest that the mafic-ultramafic cumulates were derived from a high-Mg basaltic magma. The presence of magmatic hornblende and hydrous mineral assemblages within the ultramafic cumulates indicates that the parental melts had been enriched in dissolved volatile constituents. Taking into account the age of the gabbro-norites of the Burlakski pluton (~490 ± 11.8 Ma), the magmatism likely occurred during the Ordovician collision stage of the evolution of the Central Asian Fold Belt.

Keywords: mafic-ultramafic plutons; mineral chemistry; olivine; pyroxene; hornblende; chromian spinel

1. Introduction

Numerous researchers [1–7] have focused their efforts on characterizing the petrogenesis of mafic-ultramafic intrusions, as they are ideal environments for understanding magmatic differentiation. By characterizing the primitive magma composition of a magma series, it is possible to model the composition of the rock from which a melt was formed. Moreover, Cu–Ni–platinum-group elements (PGE), Cr, and Ti ore deposits are often associated with mafic-ultramafic intrusions [8–11], so understanding how these intrusions form helps guide ore deposit exploration and extraction. Plutonic rocks of the dunite-clinopyroxenite series (dunites, wehrlites, olivine clinopyroxenites, and clinopyroxenites) are especially important as they are the main constituents of the Moho transition zone (MTZ) and their petrogenesis still remains unclear [12]. There have been many studies that have focused on dunites and clinopyroxenite xenoliths [13–16], but comparatively few studies on dunite-clinopyroxenite series rocks [14]. The main feature of the Nizhne-Derbinsk complex is the presence of ultramafic and subultramafic cumulates. The virtual absence of plagioclase in these cumulates containing both orthopyroxene and clinopyroxene, as early fractionating phases, is indicative of medium to high-pressure crystal fractionation of primary basaltic melts [17]. Our understanding of these plutons formation mechanisms, therefore, plays a critical role in understanding several petrogenetic issues such as parental and evolution of magma composition, metal and sulfur enrichment. These include the mechanism that determines the internal structure of intrusive bodies, the significance behind the various textures and structures exhibited by magmatic rocks, the mechanisms by which melts differentiate, and the development of migration pathways within intrusive bodies. Thus, according to [18–20], deep-seated mafic-ultramafic plutons relate to asthenosphere deep-lithosphere interaction processes prior to the melt-modifying processes that influence the parent melts during ascent toward the shallow crust. Moreover, these complexes have high volatile activity and they are at or close to sulfide saturation [20].

The composition of chromian spinel ($\text{Mg,Fe}^{2+}(\text{Cr,Al,Fe}^{3+})_2\text{O}_4$), is sensitive to the bulk composition, mineralogy, and petrogenesis of its host rocks and can be modified by re-equilibration with interstitial liquid, silicate minerals [21–28] hydrothermal fluids [29–34], metamorphism [30,35–37], and metasomatism [38–43]. For example, chromian spinel can be altered to Fe^{3+} -rich chromite during prograde metamorphism (amphibolite-facies) of serpentized ultramafic rocks [44] and/or by hydrothermal fluids. Chromian spinel that crystallized from mafic melts in different tectonic environments are compositionally distinct, and so their chemistry, along with the chemistry of coexisting minerals, can be a useful indicator of the former tectonic setting of mafic-ultramafic rocks [6,45]. Chromian spinel is also recognized as a sensitive mineral for characterizing the conditions that prevailed during magma crystallization [45]. Furthermore, chromian spinels have also been demonstrated to be effective tools to understand the genesis of magmatic sulfide deposits [8,10,11]. Thus, the Jinchuan intrusion [10] contains Mg-poor chromites with widely varying TiO_2 contents, showing many features that are typical of chromites in normal tholeiitic layered intrusion. Different reaction paths correlate with the abundance of sulfides in the rock.

This study provides new petrological data about two poorly studied and poorly exposed mafic-ultramafic plutons that contain dunite-clinopyroxenite series rocks. The Burlakski and Nizhne-Derbinsk plutons have long attracted the attention of researches as their mineralogical, textural, and compositional characteristics make them ideal systems to address petrological questions regarding the formation of such rarely described mafic-ultramafic systems. The petrogenesis of the Nizhne-Derbinsk mafic-ultramafic complex is still debated. Some authors [46] consider the plutons of the Nizhne-Derbinsk complex to be ophiolites related to Proterozoic magmatism, which manifested themselves in the Kuzeevsky greenstone belt. Other researchers [47] argue that the rocks of the complex are derivatives of the gabbroic-monzodioritic magmatism that occurred in the Altai-Sayan folded region. Serdyk S.S. and other geologists [48] do not exclude the fact that both Proterozoic peridotites and Ordovician gabbroic rocks are present in the Nizhne-Derbinsk complex. This contribution presents a detailed description of the rock units of the Nizhne-Derbinsk and Burlakski plutons, and combines

this information with detailed mineralogy and mineral chemistry provide a better understanding of the genesis of mafic–ultramafic systems.

2. Geological Background

2.1. Geological Setting of Plutons

The Nizhne-Derbinsk mafic-ultramafic complex is located between the Central Asian Orogenic Belt and the Siberian Craton (Figures 1 and 2a). This area is confined to the northwest part of the Eastern Sayan Mountains, roughly 100 km south of Krasnoyarsk city (Siberia, Russia) (Figure 2). The Nizhne-Derbinsk belt is roughly 40 km in length and has northeast strike. It consists of groups of spatially related plutons, including: Ashtatski, Azertakski, Burlakski, Nizhne-Derbinsk, Medvezi, Konzulski, and Tubilski (Figure 2b) [49]. Volokhov et al. [50] considered these plutons as blocks of a large single pluton. Several separate plutons, however, were mapped during geological surveying at scale of 1:50,000 [51]. The plutons are sandwiched between series of tectonic plates broken by transverse faults. Along these faults, entire blocks of different rock units are displaced. This phenomenon is manifested in various sizes of erosive section of plutons. As a result, the primary structure of the intrusive bodies is disturbed. The block structure of intrusions, as well as sometimes observed phase relationships, lead to complex relationships between individual rock types. The Nizhne-Derbinsk complex is poorly exposed with limited outcrop because of the forest cover, making it difficult to establish relationships between different rock series. According to gravity and magnetic anomalies [52], the Tubilski pluton has the form of a stock and is comprised of peridotite cumulates. It occupies an area of about 9 km². The Azertakski pluton has an ellipsoidal-shape form and contains ultramafic and subultramafic (pyroxenites) cumulates. The Ashtatkki pluton has an area of about 3 km² and is located 5 km west of the Azertakski pluton. It occurs as an oval shaped body and intruded shales of the Urman Formation. The pluton has both intrusive and tectonic contacts [50]. It consists mainly of diallagites and websterites; gabbros and peridotites, represented by wehrlites. The pluton is located in the center of the residual local gravity anomaly [52]. The Medvezi pluton has an area of about 1 km² and is located 1 km northeast of the Burlakski pluton. It has an oval shape. The Konzulski pluton is located 5 km northeast of the Burlakski pluton. The shape of the pluton is irregular with an area of 4.5 km². The pluton is composed mainly of clinopyroxenites, with lesser gabbroic rocks.

This study focuses on the Burlakski and Nizhne-Derbinsk plutons located in the central part of the complex and associated with the Ballyk fault. These plutons contain several rock types of the Nizhne-Derbinsk complex and have the potential to host Cu–Ni–PGE mineralization [49,51,53]. Within the area, there are two varieties of metamorphic rocks represented mainly by Derbinsk and Urman Formation of Proterozoic age, and non-metamorphic intrusive complexes, including Derbinsk granitoids of Proterozoic age, Buejul gabbro-monzonite-syenite-granosyenite intrusive complex of Ordovician age, and subvolcanic syenite complex of the Devonian age.

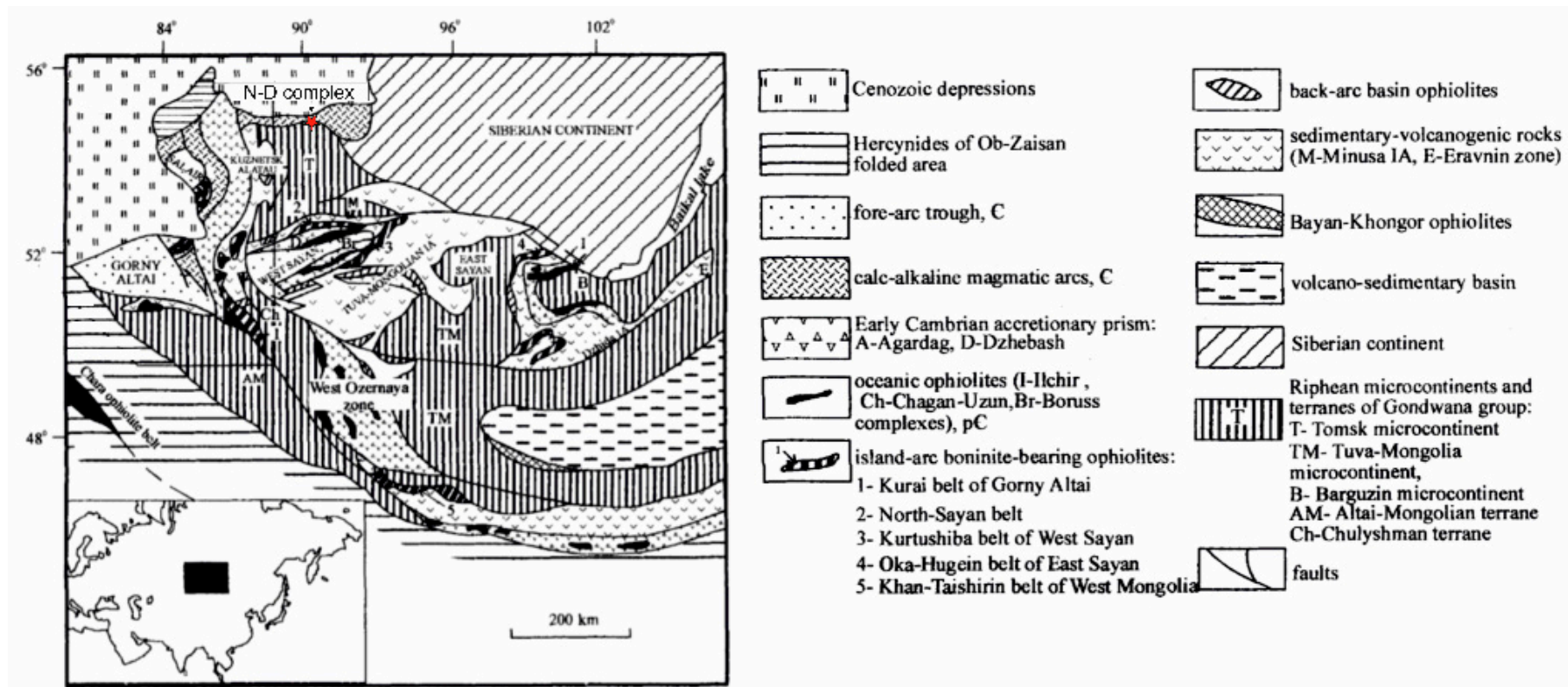


Figure 1. Geologic map of the Nizhne-Derbinsk mafic-ultramafic complex [54]. IA = Island Arc system (Tuva-Mongolian IA, Dzhida IA, Munisa IA).

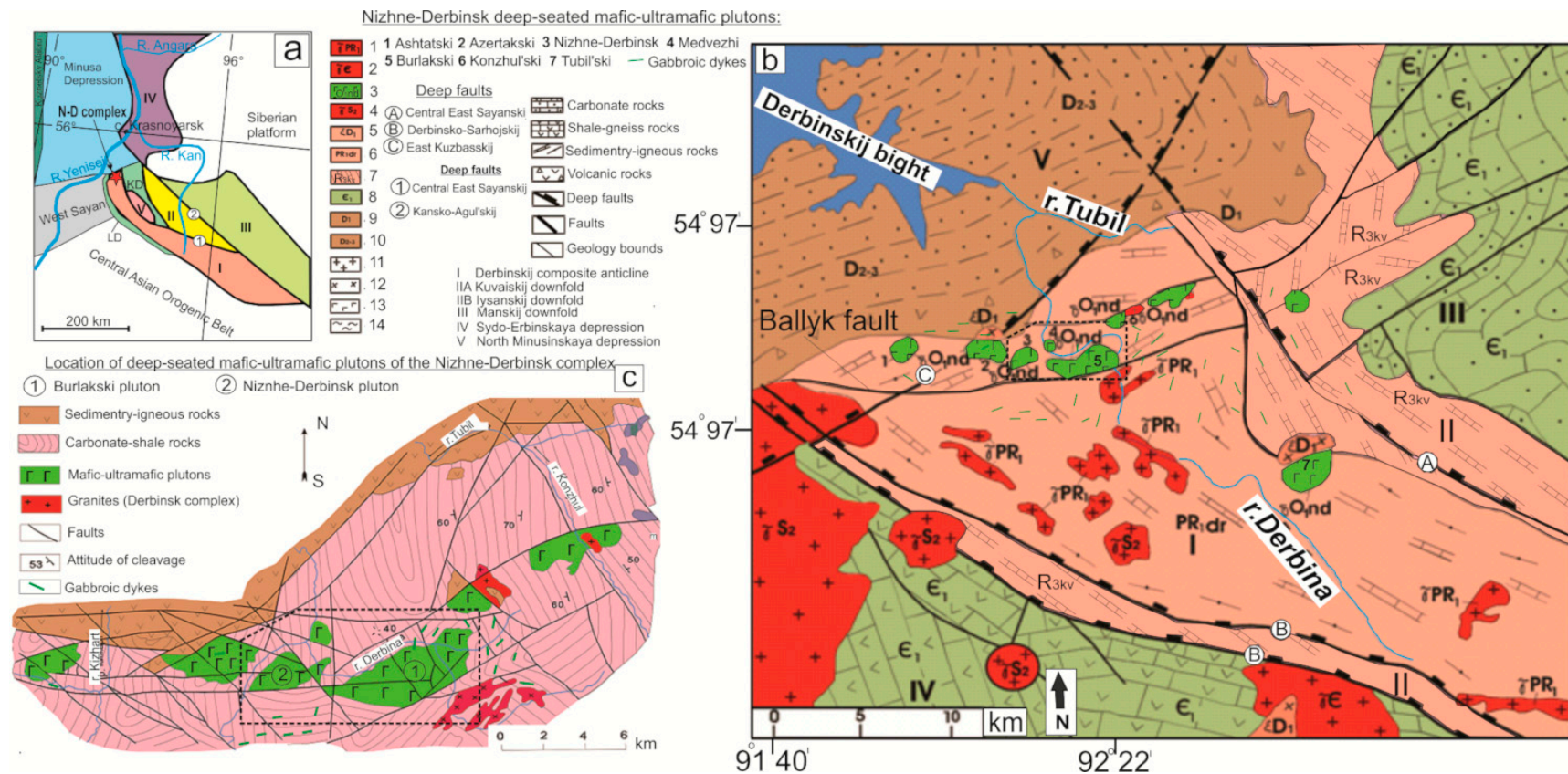


Figure 2. (a) Location of the Nizhne-Derbinsk mafic-ultramafic complex. I Derbinskiy composite anticline, II Kanskij block; crystalline basement protrusions of the Siberian platform: III Prisaynskiy, IV Angaro-Kanskij, V Azirbeyskiy; KD Kuvajskij downfold, LD Lysanskiy downfold. (b) Simplified geologic map of the Derbinsk area (East-Sayan seriya) based on the 1:200,000 regional geologic map after [53]. 1 Derbinsk granitoid complex, 2 Ballyk granitoid complex, 3 Nizhne-Derbinsk mafic-ultramafic complex, 4 Shumichinsky granitoid complex, 5 Buejulsky syenitic complex, 6 Derbinsk metamorphic Formation, 7 Kuvay metamorphic Suite, 8 Sedimentary rocks, 9 Sedimentary rocks, 10 Sedimentary rocks, 11 Granites, 12 Syenites, 13 Gabbro, 14 Spilit-diabasic Formation. (c) Location of the deep-seated mafic-ultramafic plutons of the Nizhne-Derbinsk complex (modified after [49]).

The location of emplacement of many of the Nizhne-Derbinsk plutons was controlled by the northwest- and northeast-oriented Ballyk and Kuvay fault zones [49,50]. The Precambrian crystalline basement comprises rocks of the Derbinsk and Kuvay Formation. The overlying Paleozoic sedimentary rocks are largely composed of Cambrian marble, Devonian sandy–aleuritic rocks, limestones, and marls. Intensive tectonic activity and magmatism occurred during the Proterozoic, Ordovician, and Devonian. The area of the Nizhne-Derbinsk complex belongs to the junction zone of several structures with their own stratigraphic features: Derbinsk, Kuznetsk-East Sayan, East Sayan, Minusinsk-East Sayan, and Minusinsk structural facies areas. The plutons consist of a series of tectonic slices that were cut by transverse downthrows and over faults, along which the entire blocks were displaced [49]. The Nizhne-Derbinsk complex intruded the carbonate-rich shale of the Proterozoic Derbin and Urman formations (Figure 2b,c) and was intruded by Devonian subvolcanic alkaline syenitic rocks. According to the K-Ar data of gabbro-norites from the Burlakski pluton [55] the Nizhne-Derbinsk complex is Ordovician in age ($\sim 490 \pm 11.8$ Ma) and was involved in the accretion-collisional development stage of the Central Asian fold [56].

2.2. Pluton Structure

2.2.1. Burlakski Pluton

The Burlakski pluton is located in the middle reaches of the Derbina river (Figure 2c) and occupies an area of about 16 km², making it the largest pluton of the Nizhne-Derbinsk complex. In planar view, the Burlakski pluton has a lens-like shape (5.5 × 2.5 km) with its major axis oriented roughly NE–SW. It has a vertical thickness of about 2–2.5 km according to geophysical data (vertical-component magnetics, gravity survey, electroprospecting) [51–53] and represents a lopolithic body whose contact dips toward the center at the angles ranging from 65° to 5°. In contrast, the Burlakski pluton has a cup-shaped geometry. The pluton intrudes rocks of the Urman Formation and forms aureoles of cherts, quartz-plagioclase-epidote, plagioclase-pyroxene-cordierite, garnet, and rutile that are tens of meters wide. These aureoles are most readily visible on the eastern flanks of the pluton. The rocks and structural features of the Burlakski pluton make it an ideal environment to understand the origin of the Nizhne-Derbinsk complex, because it is the largest pluton with the widest range of compositional variations. Based on the field observation data of [49,50,55] we interpreted the Burlakski pluton as a layered mafic-ultramafic body comprising serpentinites, wehrlites, pyroxenites, peridotite cumulates, and gabbroic rocks (Figure 3). The central portion of the pluton consists of the cumulate peridotite series, whereas the marginal areas comprise gabbros and gabbro-norites (Figure 3b). Dykes that crosscut the Burlakski pluton are not widely distributed and comprise both undifferentiated and differentiated rocks (Figure 2). Undifferentiated rocks include porphyritic altered gabbro-porphyrates, micro-granodiorites, and granodiorites. Differentiated rocks include spessartites and vogesites. Displacement of pluton blocks by oblique-slip faulting caused various levels of the pluton to become exposed at the surface, with the basal portions being exposed in the south-eastern and eastern parts. The basal portion of the Burlakski pluton are characterized by rhythmic layering, with layers having a thickness of 10–15 to 25–30 m of serpentinitized dunites, clinopyroxenites, and wehrlites [49], with wehrlites being the predominant rock type (section C–D in Figure 3b). Pyroxenites and serpentinites occur as lenticular bodies within the wehrlites.

Upwards in the stratigraphic sequence, pyroxenites (clinopyroxenites and websterites) that contain lens-shaped bodies of trachytic gabbro-norites occur instead of wehrlites. Wehrlites and pyroxenites generally have a massive texture and are characterized by magnetic properties. Accordingly, these rocks have been well mapped using magnetic techniques [49,51]. The magnetic properties are due to the higher content of primary magnetite and secondary magnetite that formed as a result of serpentinitization of olivine. According to field observation data of [57] the cross-cutting intrusive relationships of the ultramafic cumulates with gabbro-norites was established. A sharp crosscutting contact was observed in the northern part of Burlak Mountain: a thin pyroxenite zone (up to 2 cm) occurs at this contact. A chilled margin was detected on the side of coarse-grained gabbro-norites [57].

These observations, together with petrographic data, indicate that coarse-grained gabbro-norites are a later injection of magma. This interpretation can also explain the absence of gabbroic rocks in all other plutons of the Nizhne-Derbinsk complex.

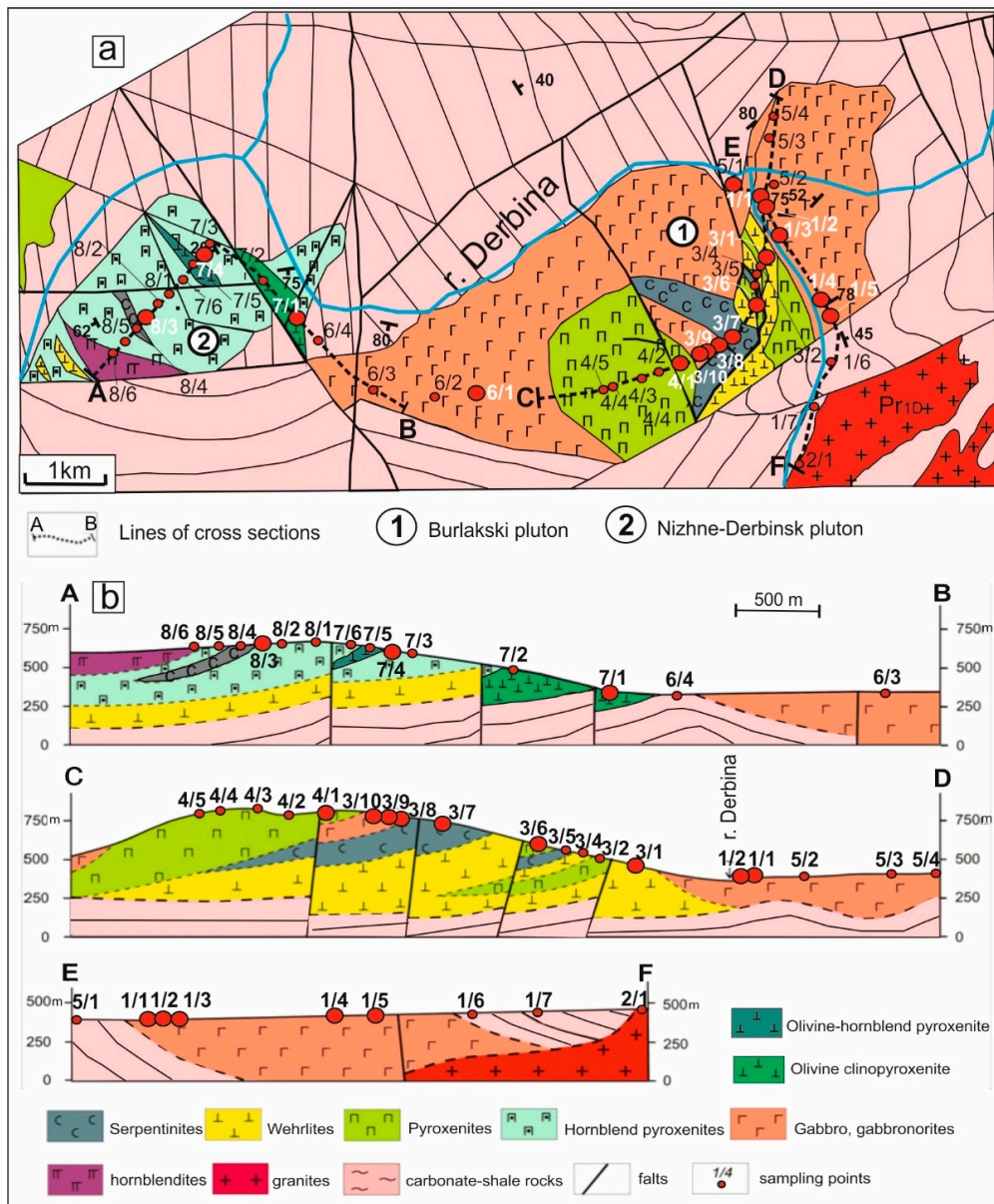


Figure 3. (a) Simplified geological map of the Burlakski (1) and Nizhne-Derbinsk (2) mafic-ultramafic plutons. (b) Simplified geological cross sections of the Nizhne-Derbinsk (A–B) and Burlakski (C–D, D–F) plutons. Big size of sampling points show where the actual outcrops occur, small size of points sampling from deluvial deposits and show where the geological map is interpreted.

Gabbro-norites of the Burlakski pluton are characterized by a well-defined trachytic texture. The gabbro-norite layers strike mainly to the northeast, and dip to the north and northwest at an angle of 45–80°, similar to the bedding of the host rocks. The orientation of the aligned plagioclase crystals typically coincides with the orientation of the layers. Izokh et al. [58] identified taxitic gabbroic rocks with large porphyritic plagioclase crystals, as well as small chert xenoliths at intrusive contacts near the right flank of the Fadeev stream (left intake of the Derbina river). Copper and Pd mineralization is confined to this contact zone [58].

2.2.2. Nizhne-Derbinsk Pluton

The Nizhne-Derbinsk pluton is located on the left flank of the Derbina River and has an area of about 4 km². The vertical thickness of the pluton does not exceed 600 m according to geophysical data [51–53]. In plain view, it has an oval shape and is elongated in the NE–SW direction (~2.7 × 2 km). The contacts of the pluton dip under it at an angle of roughly 60°, similarly to contacts in the Burlakski pluton. The pluton, which comprises wehrlites, amphibole pyroxenites, and minor hornblendites, intruded the carbonate-rich shales of the Urman Formation. Gabbroic rocks are absent.

Using previous field observations data about the internal structure of the plutons from Volokhov et al. [50] and Ekhanin et al. [49], Cherkasova and Chernyshov [59] created a schematic cross section of the Nizhne-Derbinsk pluton (Figure 2b, Section A–B). According to the cross section, we interpreted that the pluton has a layered internal structure, with wehrlites occurring at the base of the pluton and hornblende pyroxenites (clinopyroxenites and websterites) occurring in the upper portions of the pluton. Pyroxene in these rocks has typically been replaced by amphibole (uralitization and tremolitization). Small lenticular bodies (less than 100 m thick) of wehrlites were identified by [49] within the hornblende pyroxenites. The hornblendites in the southwestern part of the pluton likely represents the top of the Nizhne-Derbinsk pluton.

At the contact between the Nizhne-Derbinsk pluton and the carbonate-rich shales of the Urman Formation, the shales were metamorphosed to hornfels. Additionally, proximal to this contact, the shales and hornfels are crosscut by small dykes of granitoid rock. The granitoid melts were likely generated because of the high temperatures of contact metamorphism since granitoids are completely absent away from the contact. Similar contact melting are observed at the contact of the Chineysky massif in Transbaikalia [60], as well as the Bayankol and Bashkymugur plutons of Western Sangilen [55]. In the southwestern part of the Nizhne-Derbinsk pluton, Izokh et al. [47] identified hornfels that were crosscut by veins of fine-grained, melanocratic amphibole gabbro and granite, as well as dykes of porphyritic gabbro.

3. Materials and Methods

Thirty-seven samples of serpentinites, wehrlites, olivine clinopyroxenites, clinopyroxenites, websterites, olivine gabbro, gabbro-norites, and hornblendites from the Burlakski and Nizhne-Derbinsk plutons were collected and characterized. Given that outcrop is limited, sampling was carried out partially from outcrops and from deluvial deposits at sampling intervals of 200 m or more using a 1:25,000 topographic base map. The locations where the samples were collected are illustrated in Figure 3a. Using oriented samples, cuts were made in three mutually perpendicular directions to determine the foliation of the rocks. Polished thin sections were prepared at the Optical Laboratory of Tomsk Polytechnic University, Tomsk, Russia. The textural relationships of the minerals were characterized using a Zeiss Axio Scope A1 microscope and a TESCAN VEGA 3 SBU scanning electron microscope operated at 20 kV. Modal mineralogy (in vol. %) was estimated by point counting [61]. Quantitative chemical analyses of olivine, pyroxene, plagioclase, hornblende, and chromian spinels were collected using a Camebax-micro electron microprobe (EPMA) equipped with wavelength- and energy-dispersive spectrometers (WDS and EDS, respectively) at the Analytical Center for Multi-Elemental and Isotope Research of the Sobolev Institute of Geology and Mineralogy in Novosibirsk, Russia. Silicate minerals were analyzed using a focused beam with a spot size of 2 µm, an accelerating voltage of 20 kV, counting times of 10 s, and a beam current of 40 nA. Instrument calibration was achieved using diopside (CaKα), Mn-bearing garnet (FeKα, MnKα), Sr-bearing glass (SrLα), and Ba-bearing glass (BaLα) standards. The limit of detection for SiO₂, Al₂O₃, Na₂O, K₂O, and CaO was 0.01 wt %, and 0.02 wt % for FeO, MnO, BaO, and SrO. Chromian spinels were analyzed using a focused beam with a spot size of 2 µm, an accelerating voltage of 20 kV, counting times of 10 s, and a beam current of 50 nA. Spectral interferences were corrected for in obtaining net peak intensities. The detection limits for Ti, Al, Cr and Fe, Mn, Mg, Ni, V, and Zn were 0.014 wt %, 0.013 wt %, 0.019 wt %, 0.020 wt %, 0.010 wt %, 0.022 wt %, 0.016 wt %, and 0.039 wt %, respectively. The Fe²⁺

and Fe^{3+} contents of the spinel were estimated following the method of [62]. Cr#, Mg#, and Fe# were calculated using the atomic ratios $\text{Cr}/(\text{Cr} + \text{Al})$, $\text{Mg}/(\text{Mg} + \text{Fe}^{2+})$, and $\text{Fe}^{2+}/(\text{Mg} + \text{Fe}^{2+}) \times 100$, respectively. The two-pyroxene thermometer of [63–65] was used to characterize the crystallization temperature of the plutons. The Al^{IV} and Al^{VI} contents of pyroxene was calculated following the relationship $\text{Al}^{\text{IV}} = 2 - \text{Si}$ and $\text{Al}^{\text{VI}} = \text{Al} - \text{Al}^{\text{IV}}$.

4. Results

4.1. Petrology

4.1.1. Rocks of the Burlakski and Nizhne-Derbinsk Plutons

Rocks of the Burlakski and Nizhne-Derbinsk plutons are compositionally variable and divided into three units: peridotites, pyroxenites, and gabbroic rocks (Figure 4) [56,59]. The gabbroic rocks, however, only occur in the Burlakski pluton. The pyroxenites are the most prevalent rock type based on the current level of exposure, comprising roughly half of the outcrop area. Gabbroic rocks account for about a third of the outcrop area, with the peridotites occupying the remaining area. Although peridotites from the Burlakski and Nizhne-Derbinsk plutons both comprise wehrlites and serpentinites, they differ in that the latter contains significant amounts of hornblende.

Primary dunite and harzburgite are altered and converted to serpentinite that exhibits a cell structure and blastoporphyric texture. Serpentinites comprise lizardite (~70–80 vol. %) as pseudomorphs of olivine, magnetite (~10–30 vol. %), carbonates (~10 vol. %), bastite (up to 5 vol. %), and minor amounts (~1–5 vol. %) of chromian spinel, pyrrhotite, pentlandite, chalcopyrite, awaruite, millerite, phlogopite (Table S1, Figure 5a). In serpentinites that replaced harzburgite, the amount of bastite is greater than in those that replaced dunite, but still remains a relatively minor mineral (Figure 5a). In general, serpentinites form small horizons that are 10–30 m thick at the base of rhythmic layers that have total thickness of up to 250 m (Figure 3 section C–D). Olivine grains are 1–2 mm in size. Magnetite in the serpentinites occurs in two paragenetically distinct forms: primary magnetite I and secondary magnetite II (Figure 6), which formed as a result of serpentinization. Additionally, secondary magnetite can occur as a fine dust in serpentinite (up to 15 vol. %) (Figure 6d, Table S1).

Wehrlites are the predominant rock type of the peridotite unit in the Burlakski pluton and occur at the base of the differentiated series (Figure 2b). They comprise euhedral-subhedral olivine (~40–55 vol. %) and clinopyroxene (~40–60 vol. %) (Figure 5b). Olivine is represented by subisometric or anhedral that are 1–1.5 mm in size, sometimes up to 3 mm. Olivine are commonly serpentinized, the degree of which varies from 25% to 100%. Fragments of fresh olivine relict grains occur and are 0.2–0.4 mm in size. Clinopyroxene occurs as tabular, elongated or subisometric grains 1–3 mm in size, sometimes up to 5–10 mm. Rarely, olivine and clinopyroxene can exhibit a pokilitic texture. Sulfides include pentlandite and pyrrhotite with grain size ranging from 0.01–0.3 mm.

Olivine clinopyroxenites have an olivine content that ranges from sporadic crystals up to 20 vol. %. Pyroxenites consist of clinopyroxenites and websterites (Figure 4, Table S1). Clinopyroxenites are the dominant rock type in the Nizhne-Derbinsk complex and comprise euhedral crystals of clinopyroxene (>90 vol. %), orthopyroxene (<10 vol. %), and minor magnetite (Table S1). Clinopyroxene occurs as elongated tabular and subisometric grains ranging in size from 0.5–6.0 mm (with most having sizes between 1–2 mm). Hornblende clinopyroxenites only occur in the Nizhne-Derbinsk pluton and comprise euhedral to subhedral crystals of clinopyroxene (~85–90 vol. %), hornblende (~6–9 vol. %), magnetite (up to 4 vol. %), and pyrrhotite, chalcopyrite, and pentlandite (<5 vol. %) (Table S1).

The size of clinopyroxene grains are the same as those without hornblende. Hornblende grains have a size of about 2 mm. Biotite also occurs in the hornblende clinopyroxenites as isolated crystals up to 2.5 mm in size. Chlorite occasionally occurs as an overgrowth on biotite. Websterite is widely distributed and account for approximately 15–20 vol. % of the outcrop area of both plutons. They are composed mainly of clinopyroxene (60–90 vol. %) and orthopyroxene (up to 40 vol. %) (Figure 5c,d), but can contain olivine in abundances up to 10 vol. %. Clinopyroxene occurs as elongate or subisometric

grains ranging in size from 0.5–5.0 mm, with most being 1–2 mm. Orthopyroxene grains also exhibit a range in sizes from 0.5–4.0 mm. Orthopyroxene in the websterites contain lamellae of clinopyroxene. The websterite in the Nizhne-Derbinsk pluton is different from that in the Burlakski pluton as it contains hornblende, which occurs as anhedral grains ranging in size from 0.5–2.0 mm. Hornblendites only occur in the Nizhne-Derbinsk pluton.

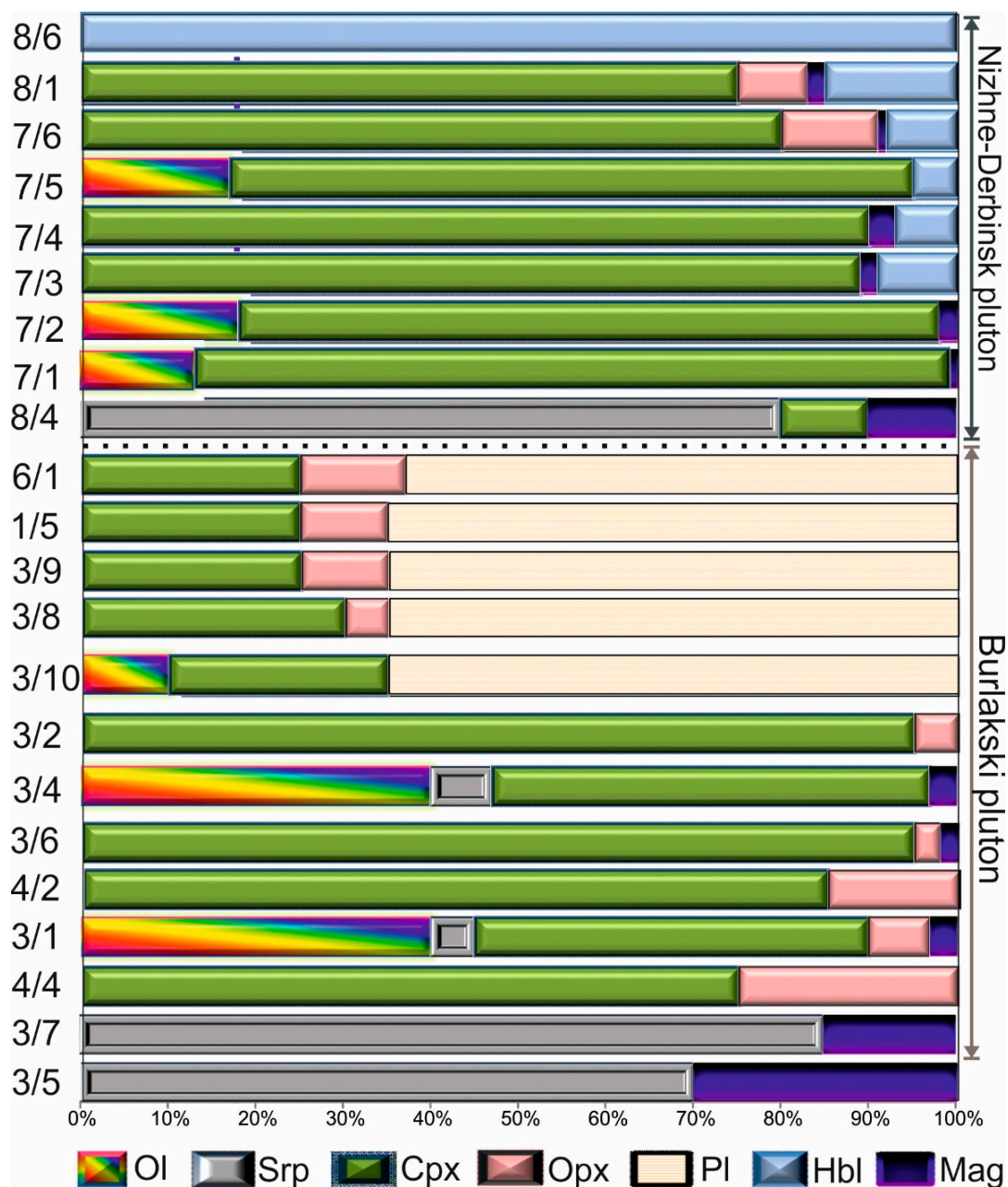


Figure 4. Mineralogy (vol. %) of the collected samples from the Burlakski and Nizhne-Derbinsk plutons represented a rough guide of stratigraphic height of these samples in the both plutons. Samples in each pluton shown in ascending order. Ol, olivine; Srp, serpentine; Cpx, clinopyroxene; Opx, orthopyroxene; Pl, plagioclase; Hbl, hornblende; Mag, magnetite.

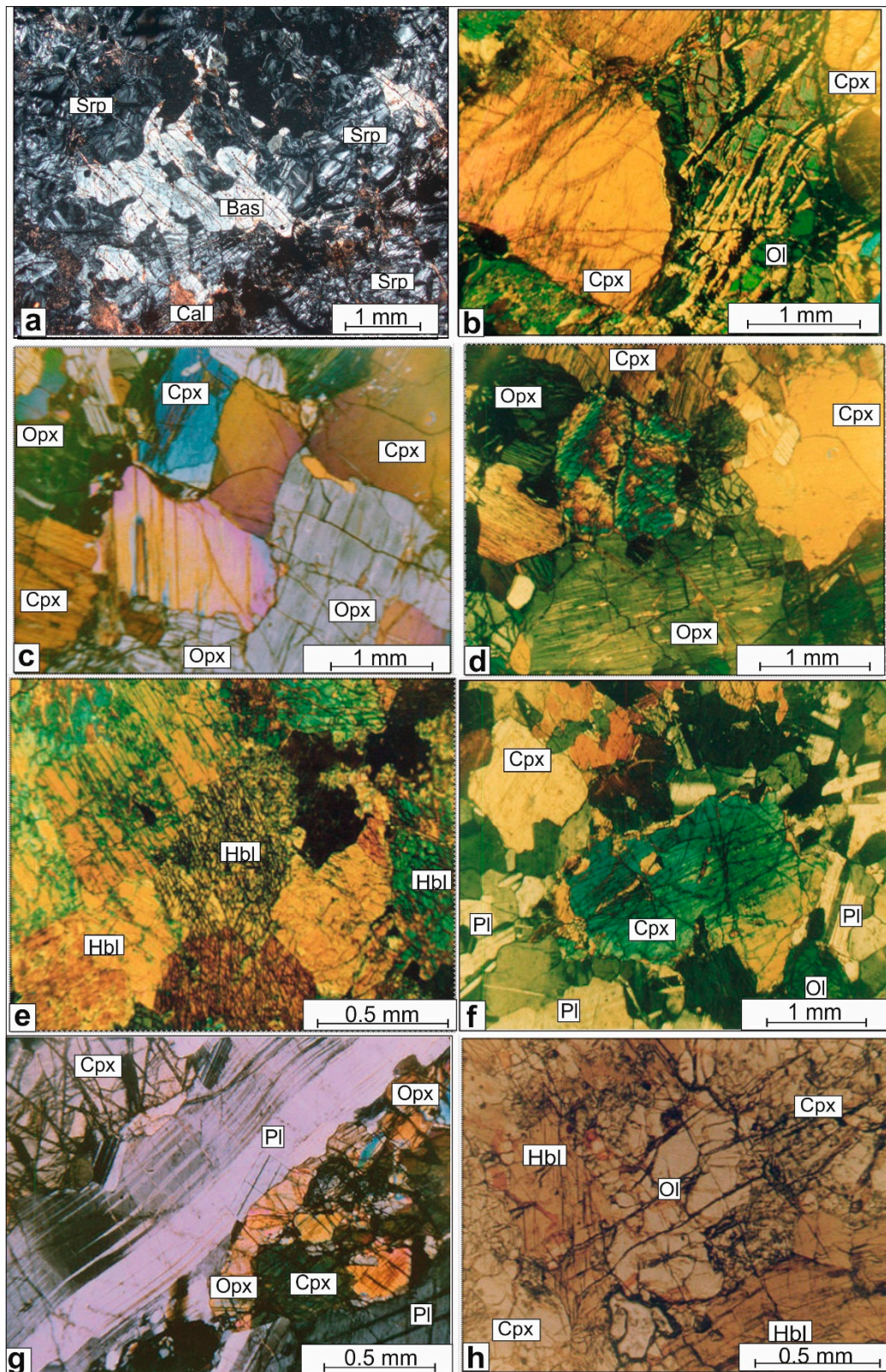


Figure 5. Transmitted-light photomicrographs in plane- and cross-polarized light. (a) Serpentine and bastite (Bas) pseudomorphs after orthopyroxene (sample 3/7). (b) Hypidiomorphic wehrlite (sample 3/1). (c) Panidiomorphic websterite (sample 4/4). (d) Poikilitic websterite (sample 4/2). (e) Panidiomorphic hornblende (sample 8/6). (f) Olivine gabbro (sample 3/10) (g) Gabbro-norite (sample 1/3) that exhibits a trachytic texture. (h) Olivine-hornblende clinopyroxenite (sample 7/5). Ol, olivine; Cpx, clinopyroxene; Opx, orthopyroxene; Pl, plagioclase; Hbl, hornblende; Srp, serpentine; Mag, magnetite.

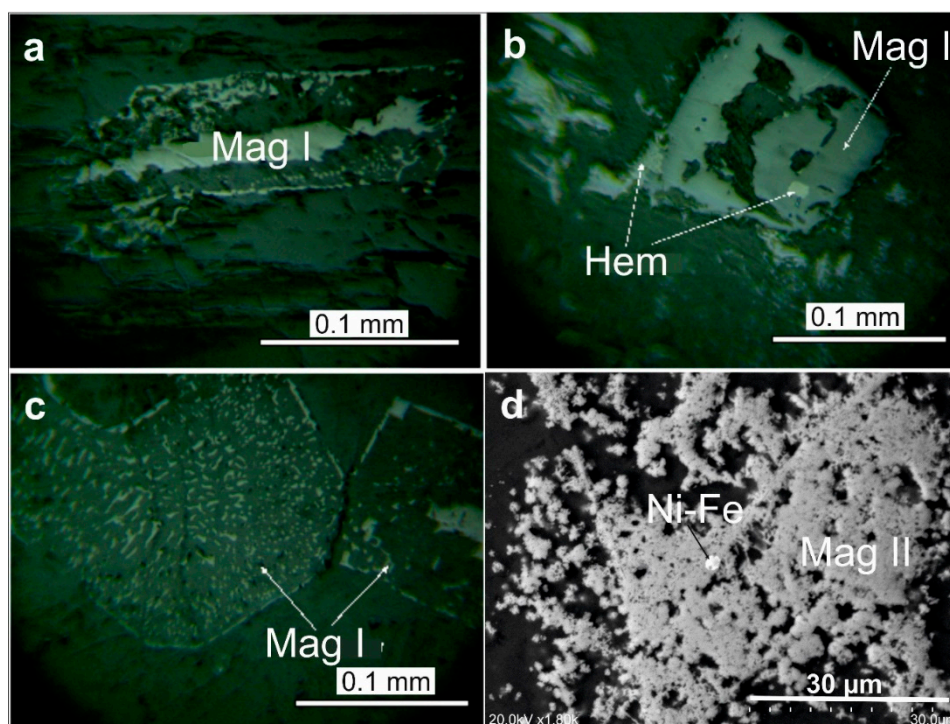


Figure 6. (a) Magnetite I that has replaced an elongated pyroxene crystal (wehrlite, sample 3/1, Burlakski pluton). (b) Isometric idiomorphic magnetite I grain replaced by later hematite (serpentinite, sample 3/7, Burlakski pluton). (c) Symplectic texture of magnetite I (wehrlite, Sample 3/1, Burlakski pluton). (d) Dusty grains of magnetite II associated with awaruite (Ni-Fe). Mag, magnetite; Hem, hematite.

The hornblendites are composed almost entirely of subisometric hornblend grains that are uniform in size and shape (~100 vol. %) (Figure 5e), with minor amounts of clinopyroxene, quartz, and plagioclase. Hornblende is represented by slightly elongated and subisometric grains. Hornblendites occur in the top layer of the Nizhne-Derbinsk pluton (see Figure 3b, Figure 5e, sample 8/6). Magmatic hornblendites were observed in other mafic-ultramafic plutons of the Central Asian Orogenic Belt [66].

Mafic rocks in the Burlakski pluton comprise gabbro and gabbro-norites (Figure 5f,g) and make up roughly 30% of the outcrop area. Anorthosites are not common in the Burlakski pluton, but do occur as separate thin layers in the leucocratic gabbro-norites. In general, the mafic rocks consist of plagioclase (~50–65 vol. %), clinopyroxene (~20–30 vol. %), and orthopyroxene (~5–15 vol. %). They can be divided into i) gabbroic rocks of the layered series that exhibit a gabbroic structure (Figure 5f) and ii) lath-shaped gabbro-norites that exhibit an ophitic texture (Figure 5g). Leucocratic olivine gabbro (Figure 5f) consists of plagioclase (~75 vol. %), clinopyroxene (~15 vol. %), olivine (~10 vol. %), biotite (~1 vol. %), and magnetite (~1 vol. %) (Table S1). These minerals are, however, irregularly distributed throughout the olivine gabbro, with some portions lacking melanocratic minerals altogether. Plagioclase in the layered series olivine gabbros occur as short, prismatic, and unzoned crystals. There are two generations of plagioclase in the gabbro-norites. The first generation of plagioclase occurs as elongate crystals that typically range in size from 2–5 mm along their longest axis, with some crystals being as long as 25 mm in the lath-shaped gabbro-norites. These elongate plagioclase crystals generally exhibit a preferred orientation.

The second generation of plagioclase, as well as clinopyroxene, and orthopyroxene are generally isometric- subisometric, characterized by a smaller grain size than first generation of plagioclase, and occur in the intervals between bands of first generation of plagioclase (Figure 5g). The first generation of plagioclase in the lath-shaped gabbro-norites are unique in that they exhibit smooth, curved crystals as a result of plastic deformation. Although pyroxene is less prone to deformation, deformation twins are observed in some crystals.

4.1.2. Mineral Description

Olivine is irregularly distributed throughout the rocks of the Burlakski and Nizhne-Derbinsk plutons, and occurs as euhedral to subhedral crystals that typically range in size from 1–1.5 mm, but can be up to 3 mm in size (Figure 5b). Most olivine crystals have been serpentinized to variable degrees ranging from 25% to 90% (Figure 5a). Fragments of relic olivine do occur, but they are small (0.2–0.4 mm in size). Fractures in olivine crystals are common and filled with lizardite (Figure 5a). Cummingtonite occasionally occurs intergrown with lizardite in these fracture fills.

Clinopyroxene is one of the dominant mineral in the ultramafic rocks of both plutons. It occurs as tabular to subisometric crystals that typically range in size from 1–3 mm (Figure 5), but can be up to 5–10 mm in size. Clinopyroxene are characterized by well-defined prismatic cleavage and twinning. The boundaries between crystals are rounded and smooth. Small crystals of clinopyroxene (<1.0 mm) are largely subisometric and can either occur interstitial to or as poikilitic inclusions within larger clinopyroxene crystals (Figure 5d). Amphibole commonly occurs as a pseudomorph after clinopyroxene (uralitization).

Orthopyroxene is irregularly distributed throughout the rocks of both plutons, ranging from as low as 3 vol. % in the clinopyroxenites to as high as 30 vol. % in websterites. In both plutons orthopyroxene crystals typically contain fine lamellae of clinopyroxene (Figure 5d). Some crystals of clinopyroxene and orthopyroxene were partially recrystallized. Large pyroxene porphyroclasts occur in a fine-grained (≤ 0.5 mm) matrix of pyroxene crystals. Brown-yellow iron hydroxides and aggregates of greenish-yellow chlorite are commonly developed along fractures in pyroxenes.

Plagioclase in gabbronorites vary in size, with porphyritic crystals ranging from 4–8 mm in length and rarely up to 25 mm. The porphyritic crystals typically exhibit a preferred orientation (i.e., flow banding) and are plastically deformed, as illustrated by their undulatory extinction and folded twin planes (see Figure 5g). In these deformed crystals, numerous simple shears have divided the porphyritic crystals into separate subgrains.

Hornblende occurs as anhedral crystals that range in size from 0.5–2.0 mm (Figure 5h). They occur as xenomorphic crystals among idiomorphic crystals of clinopyroxene or as rims on clinopyroxene (i.e., corona texture).

Chromian spinel from the Burlakski and Nizhne-Derbinsk plutons are confined to the peridotites and make up 1–3 vol. % of the rock. They occur as small (0.1–0.4 mm) euhedral, and anhedral crystals set in a matrix of serpentine (Figure 7) and pyroxene. Chromian spinel from the Nizhne-Derbinsk pluton are reddish brown to deep red in color (Figure 7a,b). Some chromian spinels contain inclusions of olivine, pyroxene, and sulfides (Figure 7c,d).

Oxides from the Burlakski and Nizhne-Derbinsk plutons are represented by magnetite I, II (Figure 6), and ilmenite.

Iron sulfides in peridotites of the Burlakski pluton consist of hexagonal pyrrhotite and troilite. The Nizhne-Derbinsk pluton contains up to 0.76% Ni. [67]. The size of pyrrhotite grains ranges from about 0.01–0.3 mm (Figure 8).

Pentlandite is less common than pyrrhotite and either occurs as flames in pyrrhotite, or as grains at the rims of the pyrrhotite (Figure 8).

Chalcopyrite is rare.

Metasomatic association within serpentinites of the Nizhne-Derbinsk complex was first described by [67]. According to the authors, metasomatic processes that actively took part in the redistribution of iron and nickel should also be involved in the redistribution of PGE + Au as confirmed by the works of, e.g., R. Larsen, M. Fiorentini, etc., [18–20] in similarly deep-seated magmatic systems.

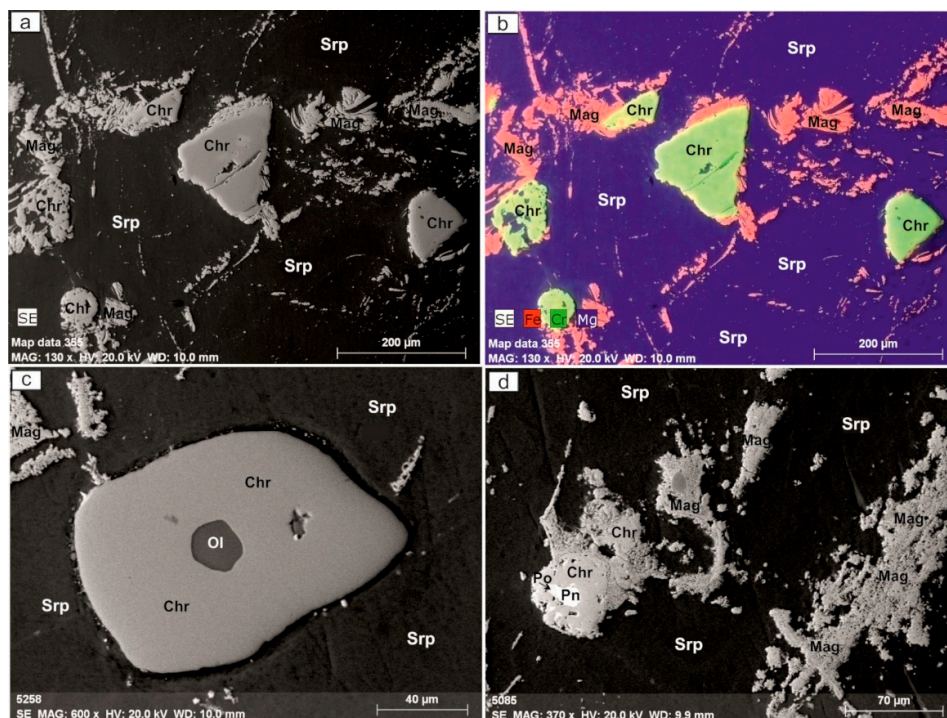


Figure 7. Backscatter electron images of chromian spinel in serpentinites of the Nizhne-Derbinsk (a,b sample 8/4) and Burlakski (c,d, sample 3/7) plutons. (a) Euhedral and subhedral crystals of chromite (Chr) adjacent to magnetite (Mag) within a matrix of serpentine (Srp). (b) Elemental map illustrating the distribution of Fe, Cr, and Mg among chromite, magnetite, and serpentine. (c) Rounded crystal of chromian spinel hosting an inclusion of olivine (Ol). (d) Anhedral crystal of chromian spinel hosting inclusions of pentlandite (Pn) and pyrrhotite (Po).

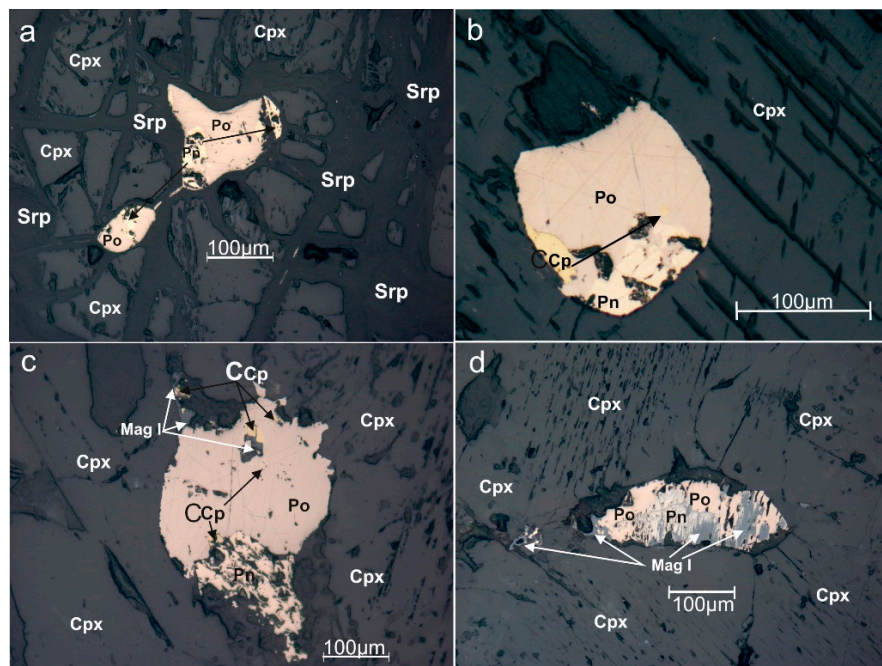


Figure 8. (a) An assemblage of pentlandite (Pn) and pyrrhotite (Po) in wehrlite (sample 3/1, Burlakski pluton). (b–d) An assemblage of chalcopyrite (Ccp)-pentlandite (Pn) and pyrrhotite (Po) in clinopyroxenite (sample 3/6, Burlakski pluton). Cpx, clinopyroxene; Srp, serpentine; Mag I, first generation magnetite.

4.2. Mineral Chemistry

Relic *olivines* in the Burlakski pluton are Mg-rich (Mg# ~85) and do not differ from relic olivine in the Nizhne-Derbinsk pluton (Mg# ~84). The main difference between olivine in these plutons is that these from the Burlakski pluton are characterized by higher nickel contents (NiO ~0.15 wt %) (Table S2).

Clinopyroxenes from both plutons have similar chemical composition (Table S3, Figure S1). Clinopyroxene in peridotites from both plutons range from augite to diopside (Table S3, Figure S1). In the Burlakski pluton, clinopyroxene in peridotites are compositionally different from those in the mafic units, with the former having lower Mg, Ni, and Cr, and higher Fe, Ti, and Na (Table S3).

Orthopyroxene in both plutons is compositionally represented by bronzite and hypersthene. They are characterized by Fe# that ranges from 18–21 wt % in the subultramafic cumulates of both plutons to 32–33 wt % in the mafic rocks of the Burlakski pluton.

Plagioclase is one of the dominant minerals in the gabbro-norites. It corresponds to labradorite with an An content of 55–57.

The chemical composition of *hornblende* in amphibole websterites from the Nizhne-Derbinsk pluton corresponds to pargasite [68] (Figure S2, Table S4).

The chemical composition of *chromian spinels* from the Burlakski pluton falls within the range of compositions of solid solution between chromite, magnesiochromite, and hercynite [69] (Table S5).

The chemical composition of chromian spinel from Nizhne-Derbinsk pluton corresponds to chromite [69]. Chromite from the Nizhne-Derbinsk pluton are characterized by a higher Cr# (~65–73) and Fe# (~72–75), and a lower Al₂O₃ (~13–16 wt %) content than chromian spinels in the Burlakski pluton (Cr# ~9–38, Fe# ~47–56 and Al₂O₃ ~24–36 wt %).

Chromian spinels in the Burlakski and Nizhne-Derbinsk plutons can be divided into three groups based on their Cr# [= Cr/(Cr + Al) × 100 atomic ratio]: type I spinels have Cr# between ~32–38, and type II spinels are characterized by Cr# between ~9–10 occur in the Burlakski intrusion, type III spinels are characterized by Cr# between ~65–75 and only occur in the Nizhne-Derbinsk intrusion. Chromian spinels in the peridotites of the Burlakski pluton above the section of the cumulate series have lower Cr# than those in the Nizhne-Derbinsk pluton.

5. Discussion

5.1. Pressure and Temperature Estimates

Estimation of the equilibrium temperature based on the Mg–Fe partition coefficients between olivine and clinopyroxene [70] revealed a temperature of formation of ~1100 °C for the Burlakski pluton and ~900 °C for the Nizhne-Derbinsk pluton. The same temperature estimates for the Nizhne-Derbinsk pluton were obtained using the olivine-spinel geothermometer [71]. Mg–Fe distribution between ortho- and clinopyroxenes may be also used for geothermometry [72], however, orthopyroxene-clinopyroxene pairs correlated with the Cr content, especially in clinopyroxenes, thus $K_D = (X_{cp} \times Mg / X_{cp} \times Fe^{2+}) \times (X_{op} \times Fe^{2+} / X_{op} \times Mg)$ within the Nizhne-Derbinsk pluton has significant variation in values and ranges from 0.9 to 1.4 (Figure S3). The large scattering of K_D is improbable according to [73] and can be explained by temperature dependence of the solubility of Cr in pyroxenes coexisting with chromian spinel [74]. According to the Ca/(Ca + Mg) of orthopyroxenes and clinopyroxenes [75] temperatures range from 1000–1382 °C. The temperatures of crystallization obtained using different pyroxene geobarometers and geothermometers [63–65] were broadly similar and, on average, range from ~1100–1400 °C (Table S6). The lower crystallization temperatures of the hornblende websterite from the Nizhne-Derbinsk pluton may be the result of amphibolization.

The virtual absence of plagioclase in ultramafic and sub-ultramafic rocks containing both orthopyroxene and clinopyroxene as early fractionating phases is indicative of medium to high-pressure crystal fractionation from primary basaltic melts [17]. According to the Al^{VI}/Al^{IV} ratio of orthopyroxenes [76], the rocks of the Burlakski and Nizhne-Derbinsk plutons crystallized at pressures ranging from 14 to 17 kb. Based on data from [77], the Al₂O₃ and Mg# number of orthopyroxenes

and clinopyroxenes fall near or within the high pressure field on the Al_2O_3 vs. Mg\# diagram of [77]. The pressures obtained from these geobarometers may reflect the conditions under which pyroxene crystallized, rather than the conditions under which the rocks crystallized. Pressure estimates using Al^{IV} and Al_{tot} content of amphiboles (Figure S4a) from [78] also indicate high pressure emplacement of the plutons, which is consistent with interpretations made using data from [79,80] (Figure S4b).

The presence of pargasite in the ultramafic rocks of the Nizhne-Derbinsk pluton and hydrous metasomatic mineral assemblages within the ultramafic cumulates of the both plutons are evidences for the enrichment of the parental melts in dissolved volatile constituents [81].

5.2. Petrological Features

According to our observations and the data of previous researchers [49,50,58], dunites and wehrlites occur at the base of the macro rhythm of the Burlakski pluton. Clinopyroxenites and websterites are recorded upsection. The central part of the macro rhythm, with a thickness of about 200 m, is composed of stratified gabbro-norites (see Figure 3). The sequence of change of rock units corresponds to the paragenesis: olivine – olivine + clinopyroxene (orthopyroxene) – clinopyroxene + orthopyroxene – clinopyroxene + orthopyroxene + plagioclase – orthopyroxene. In this sequence from ultramafic cumulates to gabbro-norites the Mg\# of olivine, clinopyroxene, and orthopyroxene ranges from 86–79, 91–72, 82–66, respectively. In the same sequence, the chemical composition of pyroxenes, as the most common minerals in both plutons there is an increase in Ti, Na, Mn. Variation in minor oxides of the pyroxenes is shown in Figure S5, where the Cr_2O_3 content of clinopyroxene increases, and Na_2O , MnO, and TiO_2 contents decrease with increasing Mg\# [= $\text{Mg}/(\text{Fe}^{2+} + \text{Mg}) \times 100\%$ atomic ratio]. Such trends are also exhibited by MnO and TiO_2 in the case of orthopyroxene. An exception is aluminum oxide Al_2O_3 .

The Cr# and Mg\# of chromian spinels in serpentinites from the Nizhne-Derbinsk pluton are negatively correlated and plot within the secondary field on the Cr# vs. Mg\# discrimination diagram of [82] (Figure 9). On the Cr_2O_3 vs. TiO_2 and Cr_2O_3 vs. Al_2O_3 discrimination diagrams of [83] and [84], many chromian spinels from the Nizhne-Derbinsk pluton plot within the stratiform pluton compositional field. In the Al–Cr– Fe^{3+} ternary diagram (Figure 10), chromian spinels from the Burlakski and Nizhne-Derbinsk plutons plot within the compositional fields for granulite and low-temperature amphibolite-facies metamorphism, respectively [71,85]. On the Cr_2O_3 vs. Al_2O_3 discrimination diagram (Figure 9f), chromian spinels from both plutons plot in the mantle array field.

Chromian spinels in both plutons have relatively high ZnO contents (up to 1.1 wt %) (Table S5), which may reflect secondary post-magmatic processes (i.e., metamorphism and serpentization) [38,39,44]. Johan and Ohnenstetter [86] suggested that the enrichment of Zn in chromian spinels may be related to their alteration by high-temperature metasomatic fluids. Such fluid involvement in the peridotite rhythms of the Burlakski and Nizhne-Derbinsk plutons is corroborated by the presence of metasomatic minerals, such as awaruite, native brass, native iron, etc., (Figure 10) [67]. Sulfide liquation is another possible cause of the higher Zn concentrations. Along with low Ni concentrations, higher Zn concentrations can be considered as an indicator of the sulfide segregation [8,87,88]. For example, chromian spinels in the upper zone of the sulfide-bearing Bushveld complex contain about 0.8 wt % ZnO, whereas those in the lower zone contain about 0.5 wt % ZnO [88]. Chromian spinels with elevated ZnO occur in the sulfide ores of Kambalda (0.53–2.92 wt %) [89] and in the sulfide deposits of the Vammala nickel belt ($\text{ZnO} > 0.8$ wt %) [88]. The ZnO contents of spinel from Jinchuan range from 0.1–1.4 wt % ZnO [10]. Chromian spinel from barren plutons in the same region as Jinchuan (e.g., the Zangbutai and Yejili plutons) typically contain less than 0.5 wt % ZnO [10].

The presence of sulfide inclusions in chromian spinels (see Figure 7d) allows assuming the potential equilibrium between the sulfide liquid and the silicate melt. The occurrence of both sulfide and silicate inclusions in chromian spinel (see Figure 7c,d) suggests that sulfide liquated early relative to the crystallization of silicates. The presence of sulfides suggests that the conditions under which these plutons formed may be favorable for the formation of Ni–Cu–PGE mineralization.

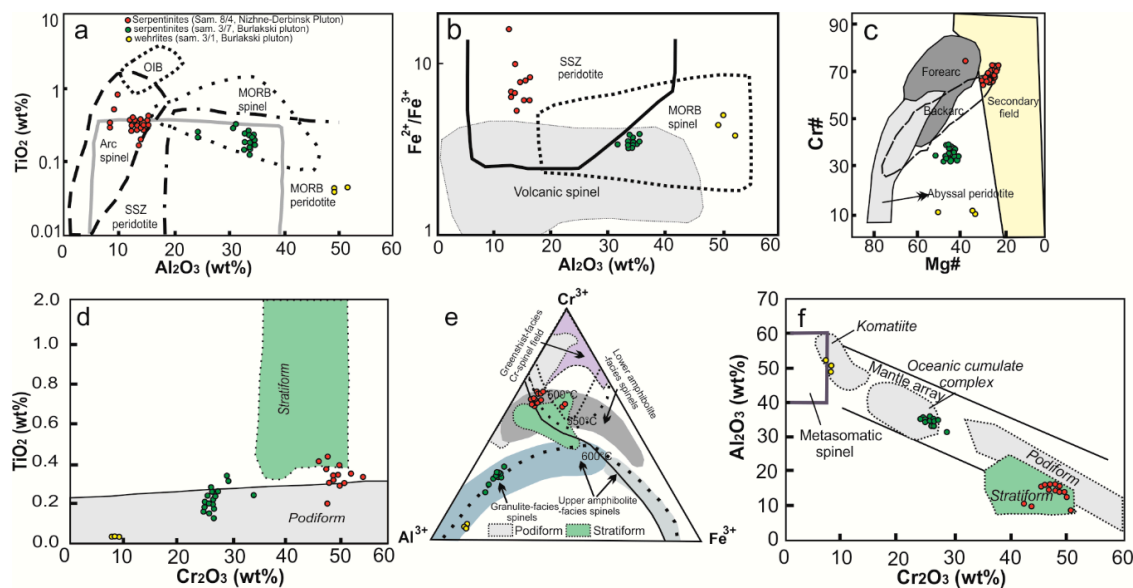


Figure 9. Binary and ternary diagrams comparing the composition of chromian spinels from the Burlakski and Nizhne-Derbinsk plutons to those from different tectonic settings. (a,b) TiO₂ vs. Al₂O₃, Al₂O₃ vs. Fe²⁺/Fe³⁺ diagrams that discriminate chromian spinel from supra-subduction zone (SSZ) and mid-ocean ridge basalt (MORB) peridotites (fields from [45]). (c) Mg# vs. Cr# diagram. The fields of abyssal and forearc peridotites is from [5]. The secondary field is from [82]. (d) Cr₂O₃ vs. TiO₂. (e) Al–Cr–Fe³⁺ ternary diagram. The spinel stability limits are from [45]. Cr–Al trend is from [6]. (f) Cr₂O₃ vs. Al₂O₃. The podiform and stratiform fields are from [83] and [84]. The field for different metamorphic facies are from [71] and [85].

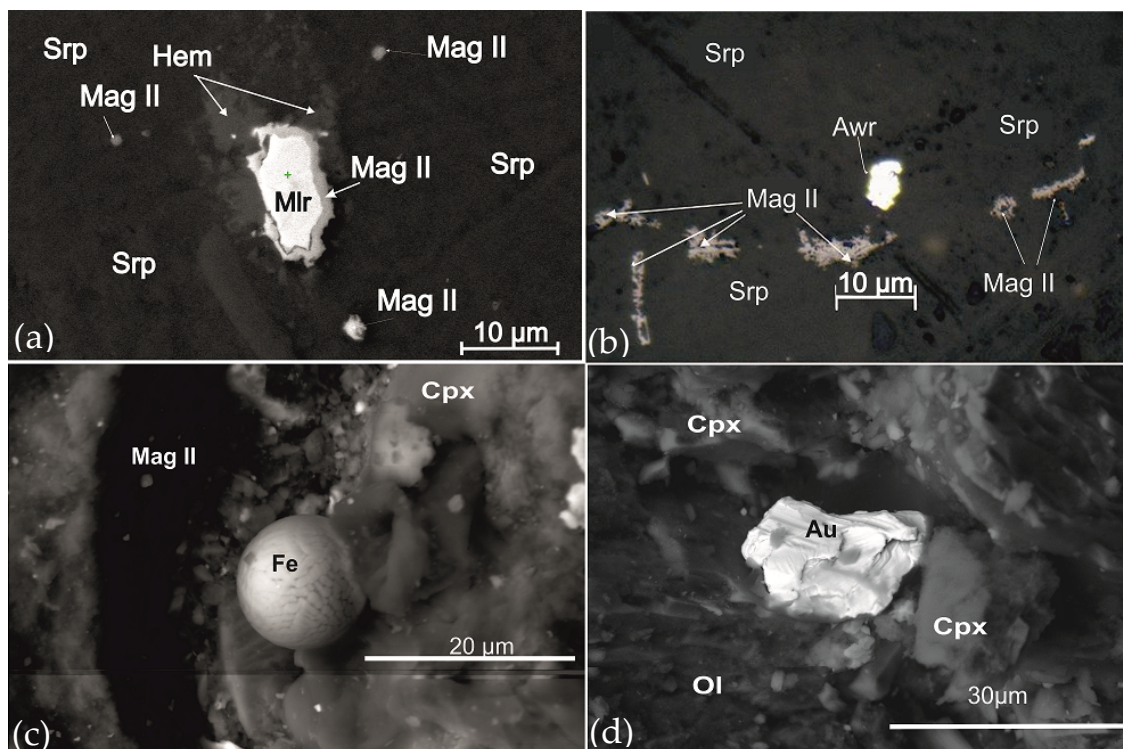


Figure 10. Backscatter electron images of (a) a millerite (Mlr) grain with a rim of magnetite II, (b) Awaruite (Awr) associated with magnetite II in the serpentinite (Srp) (sample 3/7, Burlakski pluton, (c) “spheroidal” native iron (Fe) and (d) native gold in serpentinite (Srp) of the N-D pluton (sample 8/4). Cb, carbonate.

6. Conclusions

Rocks of the main units in the Burlakski and Nizhne-Derbinsk plutons were divided into three groups: peridotites (ultramafic), pyroxenites (subultramafic), and gabbroic rocks (mafic). There are two main differences between the rock units in the Burlakski and Nizhne-Derbinsk plutons. First, the rocks from the latter contain significant amounts of hornblende and the pluton itself contains a hornblende unit. Second, the gabbro and gabbro-norite units only occur in the Burlakski pluton.

Formation of the plutons suggested by the predominance of role of the ultramafic and sub-ultramafic cumulates and a lack of more evolved rock types. Pressure and temperature estimates suggest that these plutons formed at pressures ≥ 10 kb and temperatures ranging from 1000–1400 °C. The presence of magmatic hornblende and hydrous mineral assemblages within the ultramafic cumulates indicates that the parental melts had been enriched in dissolved volatile constituents. The presence of sulfides suggests that the conditions under which these plutons formed may be favorable for the formation of Ni–Cu–PGE mineralization. Petrological and mineralogical features suggest that the rocks are mafic-ultramafic cumulates derived from a high-Mg basalt magma. Taking into account the age of the gabbro-norites of the Burlakski pluton ($\sim 490 \pm 11.8$ Ma) the magmatism likely occurred during the Ordovician collision stage of the evolution of the Central Asian Fold Belt.

Supplementary Materials: The following are available online at <http://www.mdpi.com/2075-163X/10/2/119/s1>, Figure S1. Wo-En-Fs ternary diagram illustrating the composition of clino- and orthopyroxenes in the Burlakski and Nizhne-Derbinsk plutons; Figure S2. Binary diagram illustrating the composition of hornblende in the Nizhne-Derbinsk pluton; Figure S3. Relationship of $K_D (= (X_{cp} \times Mg/X_{cp} \times Fe^{2+}) \times (X_{op} \times Fe^{2+}/X_{op} \times Mg))$ to the Cr_2O_3 contents in pyroxenes; Figure S4. (a) Al_{IV} versus $[Al]$ diagrams of natural and experimental amphiboles from [77]. (b) Al_{IV} (tot) in hornblende as function of pressure; Figure S5. Binary diagrams illustrating the variation between minor elements and $Mg\# [= Mg^{2+}/(Fe^{2+} + Mg) \times 100\%$ atomic ratio] in pyroxenes from the main rock units of the Burlakski and Nizhne-Derbinsk plutons. Table S1. Mineralogy (vol. %) of the collected samples from the Burlakski and Nizhne-Derbinsk plutons; Table S2. Major-element composition (wt%) of olivine from the Burlakski and Nizhne-Derbinsk plutons; Table S3. Major-element composition (wt%) of pyroxenes from the Burlakski and Nizhne-Derbinsk plutons; Table S4. Major-element composition (wt%) of hornblende from the Nizhne-Derbinsk pluton; Table S5. Major-element composition (wt%) of chromian spinel from the Burlakski and Nizhne-Derbinsk plutons; Table S6. Calculated temperatures and pressures of crystallization of the Burlakski and Nizhne-Derbinsk plutons based on two-pyroxene geothermobarometers.

Author Contributions: T.Y. conceived and designed the study, and wrote the initial draft of the manuscript. T.Y. and A.C. collected the samples and conducted sample preparation for analytical work. T.Y., T.T., O.S., and A.M. analyzed the data, conducted processing graphic and analytical work. M.B. and G.G. revised and corrected the final version. All authors have read and agreed to the published version of the manuscript.

Funding: This research was founded by the Russian Science Foundation with contributions from grant 16-17-10068.

Acknowledgments: Laboratory investigations were carried out at Tomsk Polytechnic University within the framework of a Tomsk Polytechnic University Competitiveness Enhancement Program grant. We thank the editors and four anonymous reviewers for their constructive criticisms and revisions, which led to the improvement of the manuscript.

Conflicts of Interest: The authors declare no conflict of interest.

References

1. Harker, A. *The Tertiary Igneous Rocks of Skye*; HM Stationery Office: Edinburgh, Scotland, 1904.
2. Bowen, N.L. *The Evolution of the Igneous Rocks*; Princeton University Press: Princeton, NJ, USA, 1928.
3. Wager, L.R.; Brown, G.M. *Layered Igneous Rocks*; Freeman: San Francisco, CA, USA, 1967.
4. Cambell, I.H.; Naldrett, A.J.; Barnes, S.J. A Model for the Origin of the Platinum-Rich Sulfide Horizons in the Bushveld and Stillwater Complexes. *J. Petrol.* **1983**, *24*, 133–165. [[CrossRef](#)]
5. Dick, H.J.B.; Bullen, T. Chromian spinel as a petrogenetic indicator in abyssal and alpine-type peridotites and spatially associated lavas. *Contrib. Mineral. Petrol.* **1984**, *86*, 54–76. [[CrossRef](#)]
6. Barnes, S.J.; Roeder, P.L. The Range of Spinel Compositions in Terrestrial Mafic and Ultramafic Rocks. *J. Petrol.* **2001**, *42*, 2279–2302. [[CrossRef](#)]
7. Borghini, G.; Rampone, E.; Crispini, L.; De Ferrari, R.; Godard, M. Origin and emplacement of ultramafic-mafic intrusions in the Erro-Tobbio mantle peridotite (Ligurian Alps, Italy). *Lithos* **2007**, *94*, 210–229. [[CrossRef](#)]

8. Zhou, M.-F.; Lightfoot, P.C.; Keays, R.R.; Moore, M.L.; Morrison, G.G.; Zhoua, M.-F.; Keays, R.R.; Lightfooe, P.C.; Morrison, G.G.; Moore, M.L. Petrogenetic significance of chromian spinels from the Sudbury Igneous Complex, Ontario, Canada. *Can. J. Earth Sci.* **1997**, *34*, 1405–1419. [\[CrossRef\]](#)
9. Jamali, H.; Yaghubpur, A.; Mehrabi, B.; Dilek, Y.; Daliran, F.; Meshkani, A. Petrogenesis and Tectono-Magmatic Setting of Meso-Cenozoic Magmatism in Azerbaijan Province, Northwestern Iran. *Petrology—New Perspectives and Applications. IntechOpen* **2012**, 39–56. [\[CrossRef\]](#)
10. Barnes, S.J.; Tang, Z.L. Chrome spinels from the Jinchuan Ni-Cu sulfide deposit, Gansu Province, People's Republic of China. *Econ. Geol.* **1999**, *94*, 343–356. [\[CrossRef\]](#)
11. Naldrett, A.; Von Gruenewaldt, G. Association of platinum-group elements with chromitite in layered intrusions and ophiolite complexes. *Econ. Geol.* **1989**, *84*, 180–187. [\[CrossRef\]](#)
12. Muroi, R.; Arai, S. Formation process of olivine-clinopyroxene cumulates inferred from Takashima xenoliths, Southwest Japan arc. *J. Mineral. Petrol. Sci.* **2014**, *109*, 79–84. [\[CrossRef\]](#)
13. Green, D.H.; Ringwood, A.E. The genesis of basaltic magmas. *Contrib. Mineral. Petrol.* **1967**, *15*, 103–190. [\[CrossRef\]](#)
14. Wandji, P.; Tsafack, J.P.F.; Bardintzeff, J.M.; Nkouathio, D.G.; Kagou Dongmo, A.; Bellon, H.; Guillou, H. Xenoliths of dunites, wehrlites and clinopyroxenites in the basanites from Batoke volcanic cone (Mount Cameroon, Central Africa): Petrogenetic implications. *Mineral. Petrol.* **2009**, *96*, 81–98. [\[CrossRef\]](#)
15. Mercier, J.C.C.; Benoit, V.; Girardeau, J. Equilibrium state of diopside-bearing harzburgites from ophiolites: Geobarometric and geodynamic implications. *Contrib. Mineral. Petrol.* **1984**, *85*, 391–403. [\[CrossRef\]](#)
16. Alifirova, T.A.; Pokhilenko, L.N.; Ovchinnikov, Y.I.; Donnelly, C.L.; Riches, A.J.V.; Taylor, L.A. Petrologic origin of exsolution textures in mantle minerals: Evidence in pyroxenitic xenoliths from Yakutia kimberlites. *Int. Geol. Rev.* **2012**, *54*, 1071–1092. [\[CrossRef\]](#)
17. Parlak, O.; Höck, V.; Delaloye, M. The supra-subduction zone Pozanti–Karsanti ophiolite, southern Turkey: Evidence for high-pressure crystal fractionation of ultramafic cumulates. *Lithos* **2002**, *65*, 205–224. [\[CrossRef\]](#)
18. Fiorentini, M.L.; LaFlamme, C.; Denyszyn, S.; Mole, D.; Maas, R.; Locmelis, M.; Caruso, S.; Bui, T.H. Post-collisional alkaline magmatism as gateway for metal and sulfur enrichment of the continental lower crust. *Geochim. Cosmochim. Acta* **2018**, *223*, 175–197. [\[CrossRef\]](#)
19. Larsen, R.B.; Grant, T.; Sørensen, B.E.; Tegner, C.; McEnroe, S.; Pastore, Z.; Fichler, C.; Nikolaisen, E.; Grannes, K.R.; Church, N.; et al. Portrait of a giant deep-seated magmatic conduit system: The Seiland Igneous Province. *Lithos* **2018**, 296–299, 600–622. [\[CrossRef\]](#)
20. Larsen, R.B.; Sørensen, B.E.; Nikolaisen, E. Formation and disruption of Cu-Ni-PGE deposits in a giant deep-seated mafic-ultramafic conduit system. In Proceedings of the 15th Biennial SGA Meeting, Glasgow, UK, 27–30 August 2019; pp. 528–531.
21. Irvine, T.N. Chromian spinel as a petrogenetic indicator: Part 1. Theory. *Can. J. Earth Sci.* **1965**, *2*, 648–672. [\[CrossRef\]](#)
22. Irvine, T.N. Chromian spinel as a petrogenetic indicator: Part 2. Petrologic applications. *Can. J. Earth Sci.* **1967**, *4*, 71–103. [\[CrossRef\]](#)
23. Liermann, H.-P.; Ganguly, J. Diffusion kinetics of Fe²⁺ and Mg in aluminous spinel. *Geochim. Cosmochim. Acta* **2002**, *66*, 2903–2913. [\[CrossRef\]](#)
24. Baumgartner, R.J.; Zaccarini, F.; Garuti, G.; Thalhammer, O.A.R. Mineralogical and geochemical investigation of layered chromitites from the Bracco–Gabbro complex, Ligurian ophiolite, Italy. *Contrib. Mineral. Petrol.* **2013**, *165*, 477–493. [\[CrossRef\]](#)
25. Dharma Rao, C.V.; Santosh, M.; Sajeev, K.; Windley, B.F. Chromite–silicate chemistry of the Neoproterozoic Sittampundi Complex, southern India: Implications for subduction-related arc magmatism. *Precambrian Res.* **2013**, *227*, 259–275. [\[CrossRef\]](#)
26. Avcı, E.; Uysal, İ.; Akmaz, R.M.; Saka, S. Ophiolitic chromitites from the Kızılyüksek area of the Pozanti–Karsanti ophiolite (Adana, southern Turkey): Implication for crystallization from a fractionated boninitic melt. *Ore Geol. Rev.* **2017**, *90*, 166–183. [\[CrossRef\]](#)
27. Xiong, F.; Yang, J.; Robinson, P.T.; Gao, J.; Chen, Y.; Lai, S. Petrology and geochemistry of peridotites and podiform chromitite in the Xigaze ophiolite, Tibet: Implications for a suprasubduction zone origin. *J. Asian Earth Sci.* **2017**, *146*, 56–75. [\[CrossRef\]](#)

28. Grieco, G.; Bussolesi, M.; Tzamos, E.; Rassios, A.E.; Kapsiotis, A. Processes of primary and re-equilibration mineralization affecting chromitite ore geochemistry within the Vourinos ultramafic sequence, Vourinos ophiolite (West Macedonia, Greece). *Ore Geol. Rev.* **2018**, *95*, 537–551. [\[CrossRef\]](#)
29. Burkhard, D.J.M. Accessory chromium spinels: Their coexistence and alteration in serpentinites. *Geochim. Cosmochim. Acta* **1993**, *57*, 1297–1306. [\[CrossRef\]](#)
30. Barnes, S.J.; Kunilov, V.Y. Spinels and mg ilmenites from the noril'sk 1 and talnakh intrusions and other mafic rocks of the siberian flood basalt province. *Econ. Geol.* **2000**, *95*, 1701–1718. [\[CrossRef\]](#)
31. Mellini, M.; Rumori, C.; Viti, C. Hydrothermally reset magmatic spinels in retrograde serpentinites: Formation of “ferritchromit” rims and chlorite aureoles. *Contrib. Mineral. Petrol.* **2005**, *149*, 266–275. [\[CrossRef\]](#)
32. Harlov, D.; Tropper, P.; Seifert, W.; Nijland, T.; Förster, H.-J. Formation of Al-rich titanite ($\text{CaTiSiO}_4\text{O}-\text{CaAlSiO}_4\text{OH}$) reaction rims on ilmenite in metamorphic rocks as a function of $f\text{H}_2\text{O}$ and $f\text{O}_2$. *Lithos* **2006**, *88*, 72–84. [\[CrossRef\]](#)
33. Mukherjee, R.; Mondal, S.K.; Rosing, M.T.; Frei, R. Compositional variations in the Mesoarchean chromites of the Nuggihalli schist belt, Western Dharwar Craton (India): Potential parental melts and implications for tectonic setting. *Contrib. Mineral. Petrol.* **2010**, *160*, 865–885. [\[CrossRef\]](#)
34. Melluso, L.; de' Gennaro, R.; Rocco, I. Compositional variations of chromiferous spinel in Mg-rich rocks of the Deccan Traps, India. *J. Earth Syst. Sci.* **2010**, *119*, 343–363. [\[CrossRef\]](#)
35. Bliss, N.W.; MacLean, W.H. The paragenesis of zoned chromite from central Manitoba. *Geochim. Cosmochim. Acta* **1975**, *39*, 973–990. [\[CrossRef\]](#)
36. Merlini, A.; Grieco, G.; Diella, V. Ferritchromite and chromian-chlorite formation in mélange-hosted Kalkan chromitite (Southern Urals, Russia). *Am. Mineral.* **2009**, *94*, 1459–1467. [\[CrossRef\]](#)
37. Gervilla, F.; Padrón-Navarta, J.A.; Kerestedjian, T.; Sergeeva, I.; González-Jiménez, J.M.; Fanlo, I. Formation of ferrian chromite in podiform chromitites from the Golyamo Kamenyane serpentinite, Eastern Rhodopes, SE Bulgaria: a two-stage process. *Contrib. Mineral. Petrol.* **2012**, *164*, 643–657. [\[CrossRef\]](#)
38. Singh, A.K.; Singh, R.K.B. Zn- and Mn-rich chrome-spinels in serpentinite of Tidding Suture Zone, Eastern Himalaya and their metamorphism and genetic significance. *Curr. Sci.* **2011**, *100*, 743–749.
39. Wylie, A.G.; Candela, P.A.; Burke, T.M. Compositional zoning in unusual Zn-rich chromite from the Sykesville District of Maryland and its bearing on the origin of “ferritchromit”. *Am. Mineral.* **1987**, *72*, 413–422.
40. Klingenberg, B.M.E.T.; Kushiro, I. Melting of a chromite-bearing harzburgite and generation of boninitic melts at low pressures under controlled oxygen fugacity. *Lithos* **1996**, *37*, 1–14. [\[CrossRef\]](#)
41. Ravikant, V.; Pal, T.; Das, D. Chromites from the Nidar ophiolite and Karzok complex, Transhimalaya, eastern Ladakh: their magmatic evolution. *J. Asian Earth Sci.* **2004**, *24*, 177–184. [\[CrossRef\]](#)
42. Arif, M.; Jan, M.Q. Petrotectonic significance of the chemistry of chromite in the ultramafic–mafic complexes of Pakistan. *J. Asian Earth Sci.* **2006**, *27*, 628–646. [\[CrossRef\]](#)
43. Gahlan, H.A.; Arai, S. Genesis of peculiarly zoned Co, Zn and Mn-rich chromian spinel in serpentinite of Bou-Azzer ophiolite, Anti-Atlas, Morocco. *J. Mineral. Petrol. Sci.* **2007**, *102*, 69–85. [\[CrossRef\]](#)
44. Barnes, S.J. Chromite in komatiites, II. Modification during greenschist to mid-amphibolite facies metamorphism. *J. Petrol.* **2000**, *41*, 387–409. [\[CrossRef\]](#)
45. Kamenetsky, V.S.; Crawford, A.J.; Meffre, S. Factors controlling chemistry of magmatic spinel: An empirical study of associated olivine, Cr-spinel and melt inclusions from primitive rocks. *J. Petrol.* **2001**, *42*, 655–671. [\[CrossRef\]](#)
46. Kornev, T.Y.; Romanov, A.P.; Knjazev, V.N.; Sharifulin, S.K. Platinum bearing greenstone belts of East Sayan Mountains and Yenisey Range. *Platinum Russia* **2004**, *5*, 358–380. (In Russian)
47. Izokh, A.; Shelepaev, R.; Lavrenchuk, A.; Borodina, E.; Yegorova, V.V.; Vasjukova, E.; Gladkochub, D. Cambro-Ordovician Variety of ultramafic-mafic associations of the Central Asian fold belt as a reflection of the interaction of the plume and lithospheric mantle. Geodynamic Evolution of the Lithosphere of the Central Asian Mobile Belt. In Proceedings of the scientific conference on the Programme of Basic Research, Irkutsk, Russia, 10–14 October 2005; pp. 106–108. (In Russian)
48. Serdyk, S.S.; Kirilenko, V.A.; Lomaeva, G.R.; Babushkin, V.E.; Tarasov, A.E.; Zverev, A.I. *Geology and Propecting Cu-Ni-PGE-Mineralization of Earst Part of Altae-Sayan Fold Mountains*; Siti: Krasnoyarsk, Russia, 2010; p. 184.

49. Ekhanin, A.; Fillipov, G.; Anikeeva, A. Geological structure features and mineralization of the Burlakski basic-ultrabasic massif (East Sayan Mountains). *Izv. Vyss. Uchebnykh Zaved. Geol. Razved.* **1991**, *9*, 72–78. (In Russian)
50. Volokhov, I.; Ivanov, V. Nizhne-Derbinsk gabbro-piroxenite-peridotite intrusive complex (Vostochnui Sayan). *Russ. Geol. Geophys.* **1964**, *5*, 52–67. (In Russian)
51. Smagin, A.N.; Nozhkin, A.D.; Homichev, V.L. *Working Correlation Scheme of Magmatic and Metamorphic Complexes of the East Sayan Mountains*; SNIIGIMS: Novosibirsk, Russia, 1997.
52. Smagin, A.N. *Magmatism and metallogeny of the Altai-Sayan folded region*; Nauka: Novosibirsk, Russia, 1971; p. 203. (In Russian)
53. Semenov, M.I.; Dolzhkovi, B.M.; Guseinov, I.F. Regional geologic map. Scale 1:200000. Seria East-Sayan. In *Sheet N-46-X*; VSEGEI: St. Petersburg, Russia, 2002; 204p. (In Russian)
54. Dobretsov, N.L.; Berzin, N.A.; Buslov, M.M. Opening and tectonic evolution of the Paleo-Asian Ocean. *Int. Geol. Rev.* **1995**, *37*, 335–360. [\[CrossRef\]](#)
55. Izokh, A.E.; Polyakov, G.V.; Mal'kovets, V.G.; Shelepaev, R.A.; Travin, A.V.; Litasov, Y.D.; Gibsher, A.A. The late Ordovician age of camptonites from the Agardag Complex of southeastern Tuva as an indicator of the plume-related magmatism during collision processes. *Dokl. Earth Sci.* **2001**, *379*, 511–514.
56. Cherkasova, T.; Chernishov, A.; Goltsova, Y.; Timkin, T.; Abramova, R. Petrogenetic characteristics of mafic-ultramafic massifs in Nizhne-Derbinsk complex (East Sayan Mountains). *IOP Conf. Ser. Earth Environ. Sci.* **2015**, *27*, 012002. [\[CrossRef\]](#)
57. Izokh, A.E. Stratified Ultramafic-Mafic Associations as Indicators of Geodynamic Settings (for Example, the Central Asian Folding Belt). Ph.D. dissertation, Sobolev Institute of Geology and Mineralogy, Novosibirsk, Russia, 1999; p. 36.
58. Izokh, A.; Kargopolov, S.; Shelepaev, R.; Travin, V.; Yegorova, V. Mafic magmatism of Cambro-Ordovician stage of the Altai-Sayan folded area and the connection of metamorphism of high temperatures and low pressures. In *Proceedings of the Actual issues of geology and minerageny of Southern Siberia*, Novosibirsk, Russia, 31 October–2 November 2001; pp. 68–72. (In Russian)
59. Cherkasova, T.; Chernyshov, A. Petrochemical characteristics of the stratified mafic-ultramafic massifs of the Nizhnederbinskiy complex (NW of the Eastern Sayan Mountains). *Tomsk. State Univ. J.* **2009**, *324*, 390–394. (In Russian)
60. Gongalsky, B.I.; Krivolutskaya, N.A.; Ariskin, A.A.; Nikolaev, G.S. The Chineysky gabbro-norite-anorthosite layered massif (Northern Transbaikalia, Russia): its structure, Fe-Ti-V and Cu-PGE deposits, and parental magma composition. *Miner. Depos.* **2016**, *51*, 1013–1034. [\[CrossRef\]](#)
61. Howarth, R.J. Improved estimators of uncertainty in proportions, point-counting, and pass-fail test results. *Am. J. Sci.* **1998**, *298*, 594–607. [\[CrossRef\]](#)
62. Droop, G.T.R. A general equation for estimating Fe³⁺ concentrations in ferromagnesian silicates and oxides from microprobe analyses, using stoichiometric criteria. *Mineral. Mag.* **1987**, *51*, 431–435. [\[CrossRef\]](#)
63. Perchuk, L.; Aranovich, L.; Kosyakova, N. Thermodynamic models of the origination and evolution of basaltic magmas. *Vestn. Mosk. Univ. Ser. Geol.* **1982**, *4*, 3–26. (In Russian)
64. Brey, G.P.; Köhler, T. Geothermobarometry in four-phase lherzolites. II. new thermobarometers, and practical assessment of existing thermobarometers. *J. Petrol.* **1990**, *31*, 1353–1378. [\[CrossRef\]](#)
65. Nimis, P.; Taylor, W.R. Single clinopyroxene thermobarometry for garnet peridotites. Part I. Calibration and testing of a Cr-in-Cpx barometer and an enstatite-in-Cpx thermometer. *Contrib. Mineral. Petrol.* **2000**, *139*, 541–554. [\[CrossRef\]](#)
66. Su, B.-X.; Qin, K.-Z.; Zhou, M.-F.; Sakyi, P.A.; Thakurta, J.; Tang, D.-M.; Liu, P.-P.; Xiao, Q.-H.; Sun, H. Petrological, geochemical and geochronological constraints on the origin of the Xiadong Ural-Alaskan type complex in NW China and tectonic implication for the evolution of southern Central Asian Orogenic Belt. *Lithos* **2014**, *200–201*, 226–240. [\[CrossRef\]](#)
67. Cherkasova, T.; Mazurov, A. Ore minerals in mafic-ultramafic rocks of Burlaksky and Nizhnederbinskiy massifs (the East Sayan). *Zap. RMO* **2012**, *141*, 77–82.
68. Hawthorne, F.; Oberti, R.; Harlow, G.E.; Maresch, W.V.; Martin, R.F.; Schumacher, J.C.; Welch, M.D. Nomenclature of the amphibole supergroup. *Am. Mineral.* **2012**, *97*, 2031–2048. [\[CrossRef\]](#)
69. Biagiony, C.; Pasero, M. The systematics of the spinel-type minerals: An overview. *Am. Mineral.* **2014**, *99*, 1254–1264. [\[CrossRef\]](#)

70. Obata, M.; Banno, S.; Mori, T. The iron-magnesium partitioning between naturally occurring coexisting olivine and Ca-rich clinopyroxene: An application of the simple mixture model to olivine solid solution. *Bull. Minéralogie* **1974**, *97*, 101–107.
71. Evans, B.W.; Frost, B.R. Chrome-spinel in progressive metamorphism—A preliminary analysis. *Geochim. Cosmochim. Acta* **1975**, *39*, 959–972. [\[CrossRef\]](#)
72. Presnall, D.C.; Dixon, S.A.; Dixon, J.R.; O'Donnell, T.H.; Brenner, N.L.; Schrock, R.L.; Dycus, D.W. Liquidus phase relations on the join diopside-forsterite-anorthite from 1 atm to 20 kbar: Their bearing on the generation and crystallization of basaltic magma. *Contrib. Mineral. Petrol.* **1978**, *66*, 203–220. [\[CrossRef\]](#)
73. Arai, S. Dunite–harzburgite–chromitite complexes as refractory residue in the sangun–yamaguchi zone, Western Japan. *J. Petrol.* **1980**, *21*, 141–165. [\[CrossRef\]](#)
74. Mysen, B.; Boettcher, A. Melting of a hydrous mantle: I. Phase relations of natural peridotite at high pressures and temperatures with controlled activities of water, carbon dioxide, and hydrogen. *J. Petrol.* **1975**, *16*, 520–548. [\[CrossRef\]](#)
75. Boyd, F. A pyroxene geotherm. *Geochim. Cosmochim. Acta* **1973**, *37*, 2533–2546. [\[CrossRef\]](#)
76. Mysen, B.O.; Kushiro, I. Compositional Variations of Coexisting Phases with Degrees of Melting of Peridotite in the Upper Mantle. *Am. Mineral.* **1977**, *62*, 843–865.
77. Medaris, J.G. High-pressure peridotites in southwestern Oregon. *Bull. Geol. Soc. Am.* **1972**, *83*, 41–58. [\[CrossRef\]](#)
78. Ridolfi, F.; Renzulli, A.; Puerini, M. Stability and chemical equilibrium of amphibole in calc-alkaline magmas: An overview, new thermobarometric formulations and application to subduction-related volcanoes. *Contrib. Mineral. Petrol.* **2010**, *160*, 45–66. [\[CrossRef\]](#)
79. Hollister, L.S.; Grissom, G.C.; Peters, E.K.; Stowell, H.H.; Sisson, V.B. Confirmation of the empirical correlation of Al in hornblende with pressure of solidification of calc-alkaline plutons. *Am. Mineral.* **1987**, *72*, 231–239.
80. Schmidt, M.W. Amphibole composition in tonalite as a function of pressure: an experimental calibration of the Al-in-hornblende barometer. *Contrib. Mineral. Petrol.* **1992**, *110*, 304–310. [\[CrossRef\]](#)
81. Metcalf, R.V.; Shervais, J.W. Suprasubduction-zone ophiolites: Is there really an ophiolite conundrum? *Spec. Pap. Geol. Soc. Am.* **2008**, *438*, 191–222.
82. Kapsiotis, A. Composition and alteration of Cr-spinels from Milia and Pefki serpentized mantle peridotites (Pindos Ophiolite Complex, Greece). *Geol. Carpathica* **2014**, *65*, 83–95. [\[CrossRef\]](#)
83. Grieco, G.; Merlini, A. Chromite alteration processes within Vourinos ophiolite. *Int. J. Earth Sci.* **2012**, *101*, 1523–1533. [\[CrossRef\]](#)
84. Mussallam, K.; Jung, D.; Burgath, K. Textural features and chemical characteristics of chromites in ultramafic rocks, Chalkidiki Complex (Northeastern Greece). *TMPM Tschermaks Mineral. Petrogr. Mitt.* **1981**, *29*, 75–101. [\[CrossRef\]](#)
85. Arai, S.; Uesugi, J.; Ahmed, A.H. Upper crustal podiform chromitite from the northern Oman ophiolite as the stratigraphically shallowest chromitite in ophiolite and its implication for Cr concentration. *Contrib. Mineral. Petrol.* **2004**, *147*, 145–154. [\[CrossRef\]](#)
86. Freitas Suita, M.T.D.; Strieder, A.J. Cr-Spinels from Brazilian Mafic-Ultramafic Complexes: Metamorphic Modifications. *Int. Geol. Rev.* **1996**, *38*, 245–267. [\[CrossRef\]](#)
87. Johan, Z.; Ohnenstetter, D. Zinco-chromite from the Guaniamo river diamond and ferrous plasers, Venezuela: Evidence of its metasomatic origin. *Can. Mineral.* **2010**, *48*, 361–374. [\[CrossRef\]](#)
88. Peltonen, P. Petrogenesis of ultramafic rocks in the Vammala Nickel Belt: Implications for crustal evolution of the early Proterozoic Svecofennian arc terrane. *Lithos* **1995**, *34*, 253–274. [\[CrossRef\]](#)
89. Paktunc, A.D.; Cabri, L.J. A proton- and electron-microprobe study of gallium, nickel and zinc distribution in chromian spinel. *Lithos* **1995**, *35*, 261–282. [\[CrossRef\]](#)

